INSTITUTE OF PHYSICS PUBLISHING JOURNAL OF PHYSICS: CONDENSED MATTER

J. Phys.: Condens. Matter **15** (2003) 6365–6380 PII: S0953-8984(03)64346-8

Structural, Mössbauer, and transport studies of the icosahedral quasicrystals $Al_{55}Si_7Cu_{25.5}Fe_{12.5}$, $Al_{62.5}Cu_{24.5}Fe_{13}$ and the crystalline 1/1 approximant $Al_{55}Si_7Cu_{25.5}Fe_{12.5}$

Zbigniew M Stadnik[1,5], **Tsunehiro Takeuchi**[2], **Nobuo Tanaka**[3] and **Uichiro Mizutani**[4]

[1] Department of Physics, University of Ottawa, Ottawa, Ontario, K1N 6N5, Canada
[2] Research Centre for Advanced Waste and Emission Management, Nagoya University, Furo-cho, Chikusa-ku, Nagoya 464-8603, Japan
[3] Centre for Integrated Research in Science and Engineering, Nagoya University, Furo-cho, Chikusa-ku, Nagoya 464-8603, Japan
[4] Department of Crystalline Materials Science, Nagoya University, Furo-cho, Chikusa-ku, Nagoya 464-8603, Japan

Received 4 June 2003
Published 8 September 2003
Online at stacks.iop.org/JPhysCM/15/6365

Abstract

As-quenched icosahedral $Al_{55}Si_7Cu_{25.5}Fe_{12.5}$, its 1/1 approximant of the same composition, and icosahedral $Al_{62.5}Cu_{24.5}Fe_{13}$ alloys have been studied using x-ray diffraction, scanning transmission electron microscopy and the high-angle annular dark field technique, zero-field and in-field ^{57}Fe Mössbauer spectroscopy, and electrical resistivity. The crystal structure of the 1/1 approximant $Al_{55}Si_7Cu_{25.5}Fe_{12.5}$ has been refined with the Rietveld method and shown to be compatible with the measured high-angle annular dark field images. The distribution of the principal component of the electric field gradient tensor has a bimodal character with a dominant negative sign in the icosahedral Al–Cu–Fe system. The local order of the Fe structural environment is compared in icosahedral $Al_{55}Si_7Cu_{25.5}Fe_{12.5}$, its 1/1 approximant, and icosahedral $Al_{62.5}Cu_{24.5}Fe_{13}$. The average quadrupole splitting decreases with temperature as $T^{3/2}$ for all alloys studied, and its value is significantly larger for the icosahedral alloys. The vibrations of the Fe atoms in the alloys studied are well described by a Debye model, with characteristic Mössbauer temperatures of 468(25), 487(19), and 455(6) K for icosahedral $Al_{55}Si_7Cu_{25.5}Fe_{12.5}$, its 1/1 approximant, and icosahedral $Al_{62.5}Cu_{24.5}Fe_{13}$, respectively. The electrical resistivity is discussed in terms of quantum interference effects and structural disorder.

[5] Author to whom any correspondence should be addressed.

1. Introduction

Quasicrystals (QCs) are a new form of solid state which differs from the other two known forms, crystalline and amorphous, in possessing a new type of long-range translational order, *quasiperiodicity*, and a noncrystallographic orientational order associated with the classically forbidden symmetry axes. A central problem in condensed-matter physics is determining whether quasiperiodicity leads to physical properties which are significantly different from those of crystalline and amorphous materials of the same/similar compositions.

The physical properties of QCs, and especially their electronic transport properties, are very unusual [1] and there has been a tendency to associate this with the quasiperiodic nature of these materials. However, it was found that equally unexpected electronic transport properties occur in the corresponding crystalline approximants to these QCs [2–4].

Physical properties of icosahedral (i) QCs in the Al–Cu–Fe system and of their approximants of the same compositions were also studied with ^{57}Fe Mössbauer spectroscopy (MS) and ^{27}Al and ^{65}Cu nuclear magnetic resonance (NMR) [5–8]. No changes in the various physical parameters measured by these techniques could be found between i-Al–Cu–Fe alloys and their approximants of the same compositions. It was concluded that local properties measured by means of ^{57}Fe MS and ^{27}Al and ^{65}Cu NMR are insensitive to the nature of the long-range order [5–8].

Recently Quivy *et al* [9] reported that an i phase forms in the quaternary system Al–Si–Cu–Fe by liquid quenching. This phase transforms into the crystalline $1/1$ approximant on annealing it at 923–953 K. Here we report on structural, zero-field and in-field ^{57}Fe MS, and electrical resistivity studies of i-$Al_{55}Si_7Cu_{25.5}Fe_{12.5}$, its $1/1$ approximant, and i-$Al_{62.5}Cu_{24.5}Fe_{13}$. The structure of the $1/1$ approximant $Al_{55}Si_7Cu_{25.5}Fe_{12.5}$ is precisely determined by the Rietveld method with great assistance from high-angle annular dark field imaging in scanning transmission electron microscopy (HAADF-STEM) experiments. We show that the distribution of the values of the electric field gradient (EFG) in these alloys has a bimodal character. The lattice vibrations of Fe atoms are well described by a simple Debye model. The much larger electrical resistivity of the i-$Al_{62.5}Cu_{24.5}Fe_{13}$ QC as compared to that of the $1/1$ approximant $Al_{55}Si_7Cu_{25.5}Fe_{12.5}$ is shown to result from structural disorder and electronic factors rather than from the quasiperiodicity of the i QC.

2. Experimental procedure

Alloy ingots of $Al_{62.5}Cu_{24.5}Fe_{13}$ and $Al_{55}Si_7Cu_{25.5}Fe_{12.5}$ were prepared from pure elements by arc melting under a pressurized argon atmosphere. All mother ingots were molten again and rapidly quenched onto a single copper roller 18 cm in diameter rotating at 5000 rpm. By annealing the quenched ribbons and ingots at 973 K for 48 h, we obtained a single-phase $Al_{55}Si_7Cu_{25.5}Fe_{12.5}$ $1/1$ cubic approximant without precipitation of any other phases. The i-$Al_{62.5}Cu_{24.5}Fe_{13}$ alloy was prepared by annealing the mother ingot and the quenched ribbons in vacuum at 973 K for 48 h.

The x-ray diffraction (XRD) spectra were measured with a Bragg–Brentano diffractometer equipped with a curved PG diffracted beam monochromator. A 0.5° divergence slit, a 0.6 mm receiving slit, and a 0.5° scatter slit were used. The XRD spectra were measured in the 2θ range 13°–140° with a step width of 0.02° using Cu Kα radiation. The Rietveld refinement of the structure of the $1/1$ $Al_{55}Si_7Cu_{25.5}Fe_{12.5}$ approximant was performed using the RIETAN program [10]. The Rietveld analysis sometimes leads to incorrect results because of the presence of many local minima in the parameter space. In order to verify that the solution found corresponds to a global minimum, we calculated the projected images from the refined

structure and compared them with the images observed in the scanning transmission electron microscopy (STEM) and high-angle annular dark field (HAADF) experiments, which were carried out with an electron microscope operated at 200 kV.

^{57}Fe MS measurements were performed in the temperature range 4.3–473.2 K using a standard Mössbauer spectrometer operating in a sine mode and a source of ^{57}Co(Rh) at room temperature. Mössbauer spectra in an external magnetic field of 9 T parallel to the γ-ray propagation direction were measured with the ^{57}Co(Rh) held at the same temperature as the sample. The spectrometer was calibrated with a 6.35 μm Fe foil [11], and the spectra were folded. Mössbauer absorbers were prepared by mixing the powdered alloys with powdered BN to ensure a uniform thickness of the absorbers and random orientation of sample particles. This mixture was then put into a plastic sample holder for low- and room-temperature measurements and into a BN holder for high-temperature measurements. The surface densities of the Mössbauer absorbers corresponding to the i-$Al_{55}Si_7Cu_{25.5}Fe_{12.5}$, its 1/1 approximant, and i-$Al_{62.5}Cu_{24.5}Fe_{13}$ were, respectively, 87×10^{-3}, 92×10^{-3}, and 94×10^{-3} mg ^{57}Fe cm^{-2}. This corresponds to an effective thickness parameter [12] at room temperature of 1.97, 2.10, and 2.08 (using the values of the absorber Lamb–Mössbauer factors of 0.823, 0.825, and 0.804 determined below), respectively. As the resulting Mössbauer spectra are due to multiple elementary quadrupole doublets, the effective thickness parameter spreads over them and therefore the absorbers can be regarded as being thin [12].

The temperature dependence of the electrical resistivity $\rho(T)$ in the temperature range 2–300 K was measured by a four-probe method using the Physical Properties Measurement System (PPMS, Quantum Design). Electrical contacts were made by gluing gold wires to the sample surface by means of silver paste. The absolute value of ρ at room temperature, $\rho_{300\ \mathrm{K}}$, was precisely determined for more than ten specimens per alloy. These precise values of $\rho_{300\ \mathrm{K}}$ were used to correct the measured values of $\rho(T)$ for the contribution from the silver paste contacts.

3. Results and discussion

3.1. Structural characterization

Figure 1 shows the XRD spectra of the as-quenched and annealed $Al_{55}Si_7Cu_{25.5}Fe_{12.5}$ alloys together with the spectrum of the i-$Al_{62.5}Cu_{24.5}Fe_{13}$ alloy. No secondary phase could be detected in the XRD spectra of i-$Al_{62.5}Cu_{24.5}Fe_{13}$ and the $Al_{55}Si_7Cu_{25.5}Fe_{12.5}$ 1/1 approximant. The presence of the i phase with some secondary crystalline phase(s) in the rapidly quenched $Al_{55}Si_7Cu_{25.5}Fe_{12.5}$ is evident in its XRD spectrum (figure 1(a)).

The atomic structure of the $Al_{55}Si_7Cu_{25.5}Fe_{12.5}$ 1/1 approximant was refined starting from the structure of the α-Al–Mn–Si phase [13] that possesses Mackay i clusters made up from doubly stacked i atomic shells with 54 atoms at the body centre and vertices of its cubic unit cell. The resulting parameters obtained in the present refinement are listed in table 1 and the refined spectrum is shown in figure 2. The accuracy of the refinement is in general judged by the overall factor R_{wp} and the structural factor R_{I}. These factors in the present analysis turn out to be sufficiently low (table 1).

The HAADF-STEM images calculated from the refined parameters reproduced the observed images well, as illustrated in figure 3. These results strongly indicate that the atomic structure of the $Al_{55}Si_7Cu_{25.5}Fe_{12.5}$ 1/1 approximant was successfully determined by the present Rietveld analysis.

Three atomic sites (M1, M8, and Mn1) in the second shell of the Mackay clusters existing at the corners of the cubic cell are filled up with a mixture of Cu and (Al, Si) in the ratio of 7:3.

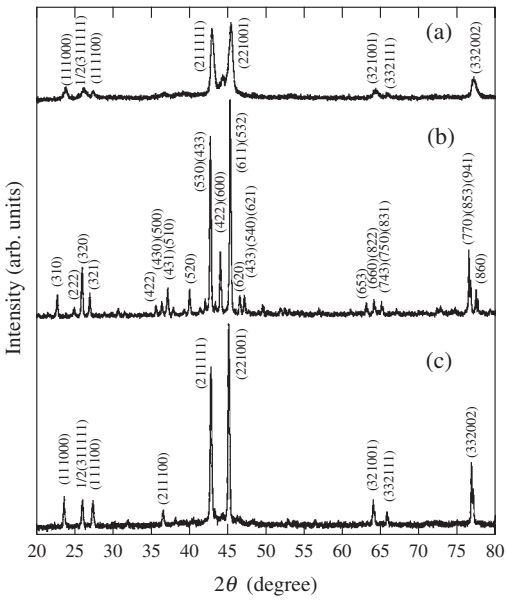

Figure 1. XRD spectra of (a) as-quenched i-$Al_{55}Si_7Cu_{25.5}Fe_{12.5}$, (b) the annealed $Al_{55}Si_7Cu_{25.5}Fe_{12.5}$ 1/1 approximant, and (c) i-$Al_{62.5}Cu_{24.5}Fe_{13}$.

Table 1. Refined structure parameters of the $Al_{55}Si_7Cu_{25.5}Fe_{12.5}$ approximant.

Space group $Pm\bar{3}$, $a = 12.321\,08(2)$ Å, M: 89 at.% Al + 11 at.% Si
$R_{wp} = 2.32$, $R_I = 3.87$, $S = 2.2966$, $R_F = 4.41$

Site	Atom	Number of atoms	Occupancy	x	y	z	B_{iso} (Å^2)
Centre	Cu	1	0.91(2)	0	0	0	0.5(4)
M1	Cu/M	6	0.70/0.30(2)	0.3697(4)	0	0	1.5(2)
M2	Cu/Fe	6	0.33/0.67(5)	0.3137(4)	0	0.5	0.52(9)
M3	M	6	1.00	0.1154(7)	0.5	0.5	0.1(1)
M4	M	12	0.36(4)	0	0.165(2)	0.090(3)	4(1)
M4′	M	6	0.14(2)	0.194(8)	0	0	2(1)
M4″	M	24	0.18(2)	0.044(2)	0.126(2)	0.149(2)	2(1)
M5	M	12	1.00	0	0.3140(5)	0.4009(5)	0.6(1)
M6	M	12	1.00	0.5	0.3345(4)	0.3991(4)	0.1(1)
M7	M	12	1.00	0.5	0.1246(5)	0.1121(6)	0.7(1)
M8	Cu/M	24	0.70/0.30(1)	0.1149(2)	0.1831(3)	0.2958(2)	1.18(7)
M9	M	24	1.00	0.3846(3)	0.3095(4)	0.1902(3)	0.1(1)
Mn1	Cu/M	12	0.72/0.28(1)	0	0.3270(3)	0.1983(3)	0.76(9)
Mn2	Fe	12	1.00	0.5	0.1788(3)	0.3030(3)	0.11(7)

These sites in the body-centre cluster, on the other hand, possess almost the same atomic arrangements as those in the α-Al–Mn–Si phase; 30 edge centres (M3 and M9) and 12 vertices (Mn2) are filled with (Al, Si) and Fe atoms, respectively. The HAADF image taken along the [100] direction clearly shows bright and dark clusters stacking in a CsCl structure. This observation clearly reflects the difference in the number of transition-metal elements between centre clusters and vertex clusters.

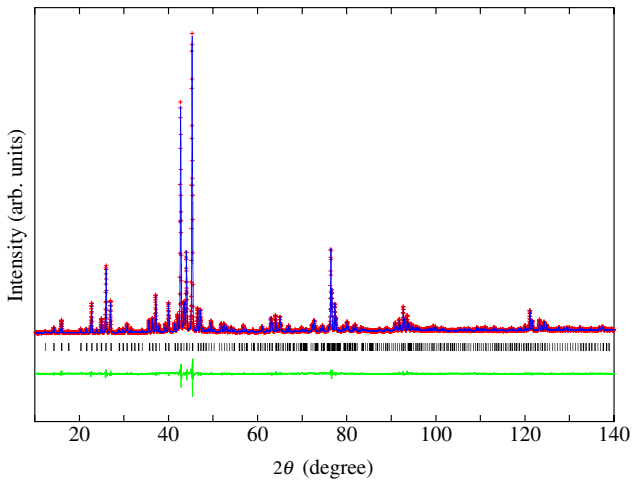

Figure 2. The Rietveld refinement pattern of the $Al_{55}Si_7Cu_{25.5}Fe_{12.5}$ 1/1 approximant. The experimental data are denoted by the red crosses, while the blue line through the data represents the results of the Rietveld refinement. The lower green curve is the difference between the experimental data and the calculated curve. The vertical bars indicate the positions of the calculated Bragg reflections.

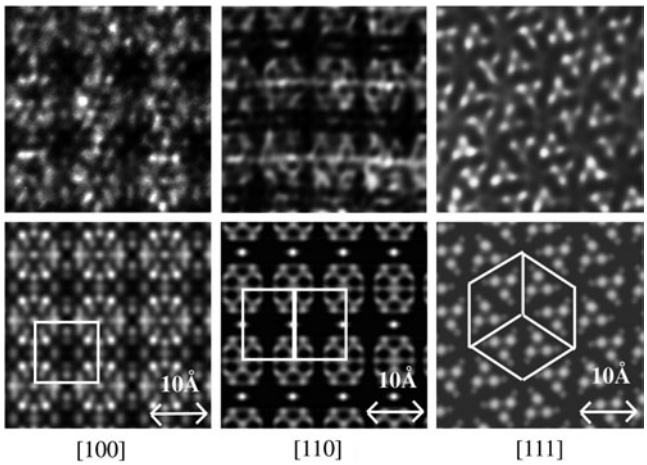

Figure 3. HAADF-STEM images taken along the [100], [110], and [111] directions. The upper panel indicates the observed images and the lower panels shows images simulated from the refined structure parameters. The white lines correspond to the edge of the cubic cell.

In addition to the heavily introduced chemical disordering between (Al, Si) and Cu, structure disordering also occurs at the M4 site that corresponds to the first atomic shell in the vertex cluster. The presence of the additionally introduced M4′ and M4″ sites and their large thermal parameters ($B_{iso} \geqslant 2$ Å^2) strongly suggest that the first shell in the vertex cluster is fairly distorted. The structure of the $Al_{55}Si_7Cu_{25.5}Fe_{12.5}$ 1/1 approximant, and perhaps that of the corresponding QC, is characterized by the presence of a similar structural disorder. The origin of this disorder was discussed by Takeuchi *et al* [14].

The Fe atoms are located at two different atomic sites in the unit cell, the Mn2 and M2 sites (table 1). The Mn2 site, which corresponds to 12 vertices on the Mackay i cluster at

corners, are fully occupied by Fe atoms. In the six positions of the M2 site, which belongs to the glue sites connecting the Mackay i clusters, Fe atoms exist together with Cu in the ratio of 2:1. Thus, 16 Fe atoms exist in the unit cell, and the Fe concentration is calculated to be $(16/136.36) \times 100 = 11.73$ at.%. The Fe concentration deduced from the refined data agrees fairly well with the nominal one of 12.5 at.% Fe.

The structure of the Al–Cu–Fe–Si 1/1 cubic approximant was recently determined by Puyraimond *et al* [15] on the basis of the analysis of single-crystal XRD data. Their resulting R factor (4.15%), which corresponds to the R_F factor in the Rietveld analysis, is almost the same as $R_F = 4.41\%$ (table 1) obtained by us. This indicates comparable reliability of the structure parameters. The positions of the atomic sites in these two independent studies show a fairly good agreement. Indeed, the presence of the strong chemical disorder between Al and Cu at the M1 and M8 sites is also shown in the result of Puyraimond *et al* [15]. However, the differences between our result and that of Puyraimond *et al* are as regards (a) the M4 site, where we intentionally introduced additional M4′ and M4″ sites, and (b) the atomic sites occupied only by Fe atoms.

The difference (a) can be explained by the presence of a strong disorder at the M4 sites. In our analysis, this strong disorder is dealt with by introducing additional atomic positions M4′ and M4″, whereas Puyraimond *et al* account for it through an extraordinarily large thermal parameter $B_{eq} = 13.9$ Å^2. The difference (b) is a more serious problem. In our analysis, Fe atoms occupy only the Mn2 and M2 sites, whereas they are distributed over five different sites according to Puyraimond *et al* [15]. Puyraimond *et al* [15] comment on this difference, referring to our preliminary study [16], by noting that since the two structural models give almost the same local electron density, it is difficult to conclude which model is the right one. The closeness of the atomic numbers of Cu and Fe makes the case even more difficult to solve. We note, however, that we have recently determined, with synchrotron radiation XRD, the structure of the $Al_{54}Si_8Cu_{25.5}Ru_{12.5}$ 1/1 cubic approximant [17], which is obtained by replacing Fe atoms in $Al_{54}Si_8Cu_{25.5}Fe_{12.5}$ with Ru atoms. As the atomic number of Ru is much larger than that of Cu, the analysis of the high-quality synchrotron radiation XRD spectrum allowed us to precisely determine the positions of the Ru atoms in the $Al_{54}Si_8Cu_{25.5}Ru_{12.5}$ 1/1 cubic approximant, yielding the R_F factor of 1.18% [17]. This analysis shows that Ru atoms occupy only two sites [17], which are the same as the sites occupied by Fe atoms in the $Al_{55}Si_7Cu_{25.5}Fe_{12.5}$ 1/1 cubic approximant studied here. We therefore strongly believe that Fe atoms do indeed occupy only the two sites Mn2 and M2 in the $Al_{55}Si_7Cu_{25.5}Fe_{12.5}$ 1/1 cubic approximant. Additional evidence for the presence of the Fe atoms only at the two sites comes from the analysis of the in-field Mössbauer spectra discussed below.

3.2. Mössbauer spectroscopy

Low-temperature Mössbauer spectra of the i-$Al_{55}Si_7Cu_{25.5}Fe_{12.5}$, its 1/1 approximant, and i-$Al_{62.5}Cu_{24.5}Fe_{13}$ (figures 4(a)–(c)), similarly to the spectra of other nonmagnetic i alloys [18], consist of a broadened asymmetric doublet which results from the distribution $P(\Delta)$ of the quadrupole splitting

$$\Delta = \tfrac{1}{2} e Q |V_{zz}| (1 + \tfrac{1}{3}\eta^2)^{1/2}, \tag{1}$$

where e is the proton charge and Q is the electric quadrupole moment of the nucleus. The asymmetry parameter $\eta = (V_{xx} - V_{yy})/V_{zz}$ $(0 \leqslant \eta \leqslant 1)$, where V_{xx}, V_{yy}, and V_{zz} are the eigenvalues of the EFG tensor in order of increasing magnitude [12]. The distribution $P(\Delta)$ is the consequence of the distributions of the EFG and of the asymmetry parameter. The fits of the spectra in figure 1 give information on the magnitude of Δ, but not on the sign of the

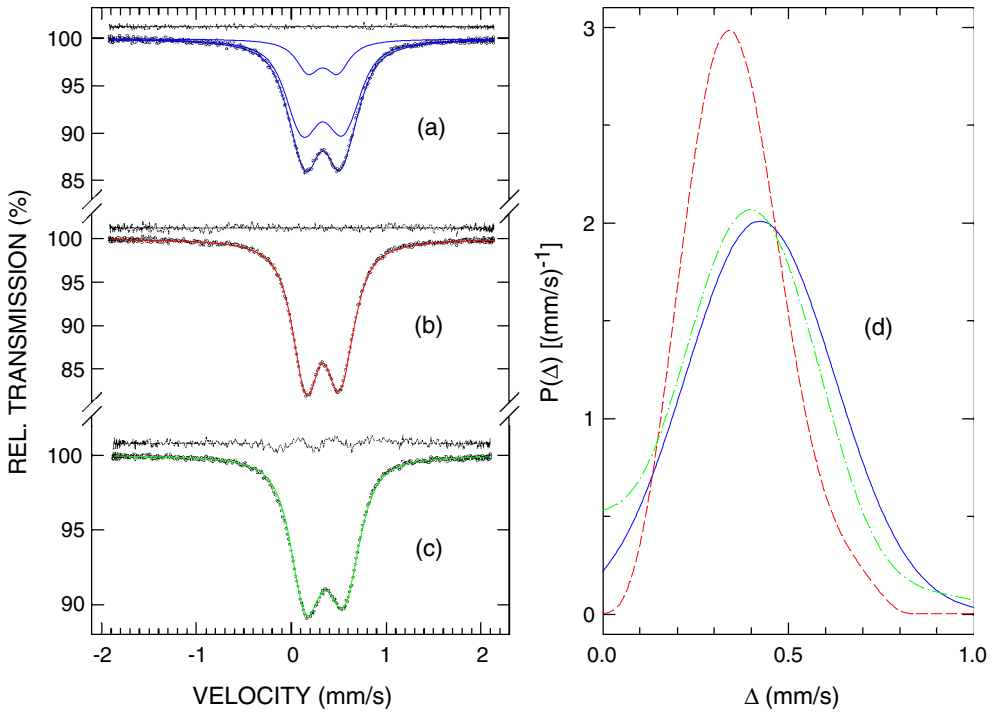

Figure 4. ^{57}Fe Mössbauer spectra of (a) i-$Al_{55}Si_7Cu_{25.5}Fe_{12.5}$ at 4.6 K fitted (solid curve) with the impurity and $P(\Delta)$ components, (b) its 1/1 approximant at 4.4 K, and (c) i-$Al_{62.5}Cu_{24.5}Fe_{13}$ at 4.3 K fitted (solid curve) with the distributions $P(\Delta)$ shown in (d) (solid, dashed, and dot–dashed curves, respectively). The zero of the velocity scale in (a)–(c) is relative to α-Fe at room temperature. The residuals are shown above each spectrum.

main component of the EFG, V_{zz}, or the value of η. Complete information on the sign of V_{zz} and the value of η can be obtained from spectra measured in external magnetic fields such that the magnetic dipole interaction becomes of similar magnitude to the electric quadrupole interaction.

The low-temperature Mössbauer spectra in figure 4 were fitted with the constrained version [19] of the Hesse–Rübartsch method [20]. A slight asymmetry of the spectra was accounted for by assuming a linear relation between the centre shift, δ, and Δ for the elementary Lorentzian doublets of full width at half-maximum Γ [18]. A small distribution of δ, independent of the EFG, was assumed and characterized by the standard deviation parameter σ_δ. The spectrum of the i-$Al_{55}Si_7Cu_{25.5}Fe_{12.5}$ sample ((figure 4(a)), which contains a significant fraction of the second phase, could be fitted successfully with only two components corresponding, respectively, to the impurity phase and the i phase. Satisfactory fits, as judged by the values of χ^2 and by the residuals (figures 4(a)–(c)), were obtained for the distributions $P(\Delta)$ shown in figure 4(d). The parameters obtained from the fits are given in table 2.

The presence of a wide distribution $P(\Delta)$ for the alloys studied indicates the presence of quasicontinuous distributions of local environments in the alloys studied. The Rietveld analysis of the XRD spectrum of the 1/1 approximant indicates that the Fe atoms are located at two sites, Mn2 and M2. This should, in principle, be reflected in the double-peak structure of the $P(\Delta)$ distribution. The fact that this distribution is single peaked and almost symmetric indicates that the zero-field Mössbauer spectra of alloys with complex unit cells containing

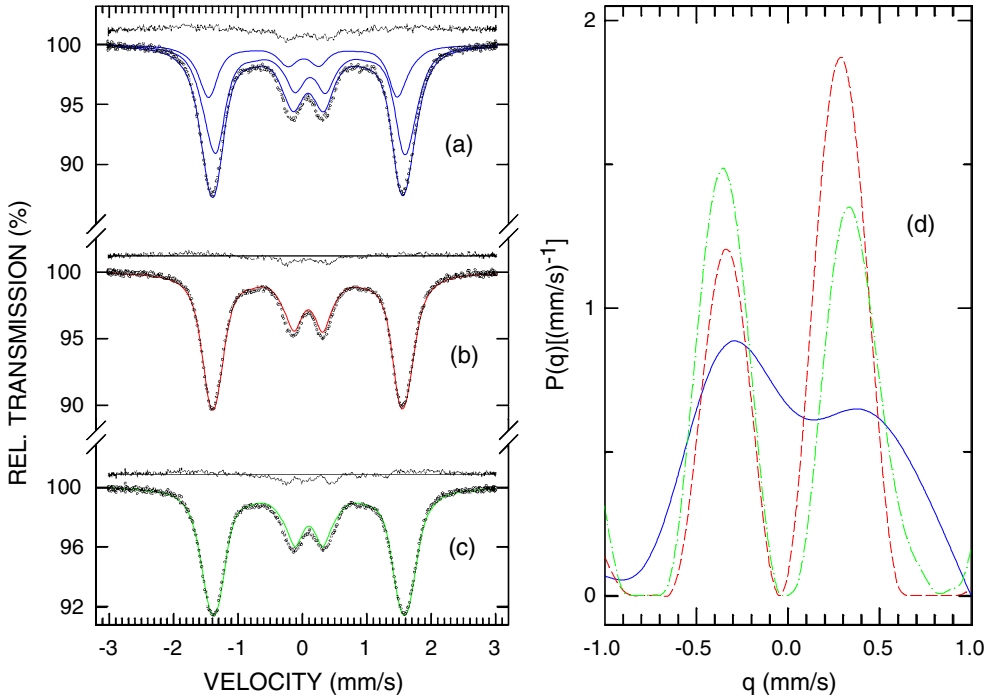

Figure 5. ^{57}Fe Mössbauer spectra measured in an external magnetic field of 9.0 T of (a) i-$Al_{55}Si_7Cu_{25.5}Fe_{12.5}$ at 5.5 K fitted (solid curve) with the impurity and $P(q)$ components, (b) its 1/1 approximant at 5.4 K, and (c) i-$Al_{62.5}Cu_{24.5}Fe_{13}$ at 4.4 K fitted (solid curve) with the distributions $P(q)$ shown in (d) (solid, dashed, and dot–dashed curves, respectively). The zero of the velocity scale in (a)–(c) is relative to the ^{57}Co(Rh) source at the same temperature as the absorber. The residuals are shown above each spectrum.

Table 2. Hyperfine parameters obtained from the fits of the low-temperature ^{57}Fe Mössbauer spectra in figures 4(a)–(c): $\bar{\delta}$ is the average centre shift (with respect to α-Fe at room temperature), its standard deviation is $\sigma_{\bar{\delta}}$, $\bar{\Delta}$ is the average quadrupole splitting, its standard deviation is $\sigma_{\bar{\Delta}}$, and Γ is the full width at half-maximum of the elementary Lorentzian doublets.

Sample	T (K)	$\bar{\delta}$ (mm s^{-1})	$\sigma_{\bar{\delta}}$ (mm s^{-1})	$\bar{\Delta}$ (mm s^{-1})	$\sigma_{\bar{\Delta}}$ (mm s^{-1})	$\bar{\Delta}/\sigma_{\bar{\Delta}}$	Γ (mm s^{-1})
i-$Al_{55}Si_7Cu_{25.5}Fe_{12.5}$	4.6	0.3301(41)	0.0019(1)	0.4155(9)	0.1909(10)	2.177(16)	0.2947(8)
1/1 approximant $Al_{55}Si_7Cu_{25.5}Fe_{12.5}$	4.4	0.3324(26)	0.0039(2)	0.3639(9)	0.1330(17)	2.736(42)	0.2672(7)
i-$Al_{62.5}Cu_{24.5}Fe_{13}$	4.3	0.3493(18)	0.0054(3)	0.3961(14)	0.1954(24)	2.027(31)	0.2472(5)

two (or more) inequivalent Fe sites cannot be used to confirm the presence of such sites. The $P(\Delta)$ distributions of the i alloys $Al_{55}Si_7Cu_{25.5}Fe_{12.5}$ and $Al_{62.5}Cu_{24.5}Fe_{13}$ (figure 4(d)) are almost the same, which means that the local atomic structures around the Fe atoms in these two alloys are virtually identical. The $P(\Delta)$ distribution corresponding to the 1/1 approximant $Al_{55}Si_7Cu_{25.5}Fe_{12.5}$ (figure 4(d)) is narrower and shifted towards the lower values of Δ, but its shape is similar to the $P(\Delta)$ distributions corresponding to the i alloys. This indicates that the local atomic structures around the Fe atoms are very similar in these alloys.

To determine the sign of V_{zz} and the value of η for the alloys studied, Mössbauer spectra were measured in an external magnetic field of 9 T (figures 5(a)–(c)). The Mössbauer spectra

exhibiting mixed hyperfine magnetic dipole and electric quadrupole interactions must be treated using the exact Hamiltonian [12]. If texture effects are negligible one can assume, similarly to the case for powder samples, that the principal axes of the EFG tensor are randomly oriented with respect to the external magnetic field. The algorithm for calculating the spectra in such a case was given by Blaes *et al* [21] and was used to fit the spectra in figures 5(a)–(c). As the ^{57}Fe Mössbauer spectra are of very limited sensitivity to the distribution of η, and are mainly sensitive to its average value $\bar{\eta}$ [22], the fits of the spectra in figures 5(a)–(c) were carried out for one value of $\bar{\eta}$ and the distribution $P(q)$, where $q = \frac{1}{2}eQV_{zz}$. The distributions $P(q)$ derived from the fits are shown in figure 5(d) and the parameters obtained from the fits are given in table 3.

The distributions $P(q)$ are bimodal in character (figure 5(d)) with a predominantly positive sign of V_{zz} for the i-$Al_{55}Si_7Cu_{25.5}Fe_{12.5}$ alloy and its 1/1 approximant, and a predominantly negative sign of V_{zz} for the i-$Al_{62.5}Cu_{24.5}Fe_{13}$ alloy. The bimodal nature of the distribution $P(q)$ for the 1/1 approximant (figure 5(d)) points to the existence of two nonequivalent classes of Fe sites in the structure of this alloy. This is consistent with the result of the Rietveld analysis of the XRD spectrum of this alloy which indicates that the Fe atoms are located at two sites, Mn2 and M2, with the occupancies, respectively, of 1.0 and 0.67. Thus, the Fe atoms with a positive sign of V_{zz} are located at the Mn2 site, whereas those with a negative sign of V_{zz} are situated at the M2 site.

The distribution $P(q)$ for the i-$Al_{55}Si_7Cu_{25.5}Fe_{12.5}$ alloy (figure 5(d)) is similar to that for the 1/1 approximant; the main differences lie in significantly larger widths of the two components with their peaks shifted towards the larger q values. The similarity in shape of the $P(q)$ distributions for these two alloys indicates that, not surprisingly, the geometry of the local structure around the Fe atoms in the i-$Al_{55}Si_7Cu_{25.5}Fe_{12.5}$ alloy is close to that of its 1/1 approximants. The shift of the q-peak values indicates that the distances between Fe and its nearest-neighbour atoms in the i-$Al_{55}Si_7Cu_{25.5}Fe_{12.5}$ alloy are slightly different to those in the 1/1 approximant, whereas the broader components indicate the presence of more topological disorder in the i-$Al_{55}Si_7Cu_{25.5}Fe_{12.5}$ alloy than in its 1/1 approximant.

The shape of the distribution $P(q)$ for the i-$Al_{62.5}Cu_{24.5}Fe_{13}$ alloy is almost identical to that for the 1/1 approximant $Al_{55}Si_7Cu_{25.5}Fe_{12.5}$ (figure 5(d) and table 3); the only difference is the reversal of the double-peak probability. The double-peak distribution $P(q)$, with a predominantly negative sign of V_{zz}, is thus a signature of the i structure in the Al–Cu–Fe system.

The distribution $P(q)$ is directly related to the local atomic structure [18]. In principle, the experimentally determined distribution $P(q)$ could be used to narrow down the possible structural models for the i alloys Al–Cu–Fe and Al–Si–Cu–Fe [23]. This would require band-structure calculations of the EFG tensor for a given structural model, which is a challenging endeavour [24, 25] . Recently, Zijlstra *et al* [26] carried out *ab initio* density functional calculations of the density of states and of the EFGs for the model of i-Al–Cu–Fe due to Cockayne *et al* [27], which is based on the synchrotron radiation XRD data from single-grain i-Al–Cu–Fe [28]. In this model, Fe atoms occupy two crystallographic sites. Zijlstra *et al* [26] find the values of η and q at these sites equal to 0.7, 0.31 mm s^{-1} and 0.0, 0.29 mm s^{-1}. This is clearly at variance with the values determined experimentally for i-$Al_{62.5}Cu_{24.5}Fe_{13}$ (table 3) of 0.0, 0.37 mm s^{-1} and 0.0, -0.38 mm s^{-1}. Zijlstra *et al* [26] improve the Cockayne model by using forces determined from *ab initio* density functional calculations instead of forces based on empirical pair potentials to relax the atomic positions. For this relaxed Cockayne model they obtain η and q at the two Fe sites equal to 0.6, 0.20 mm s^{-1} and 0.0, -0.08 mm s^{-1}. Although the absolute values of the calculated q differ significantly from the experimental ones, clearly the relaxed Cockayne model accounts for the negative and positive q, i.e. for the

Table 3. Hyperfine parameters obtained from the fits of the low-temperature ^{57}Fe Mössbauer spectra in figures 5(a)–(c): $\bar{\delta}$ is the average centre shift (with respect to the ^{57}Co(Rh) source at the same temperature as the sample) over the positive and negative distributions $P(q)$, $\sigma_{\bar{\delta}}$ is its standard deviation, $\bar{q}_+$ and $\bar{q}_-$ are the averages of q, respectively, over the positive and negative $P(q)$, $\sigma_{\bar{q}_+}$ and $\sigma_{\bar{q}_-}$ are the corresponding standard deviations, $\bar{\eta}$ is the average asymmetry parameter, p_+ is the fraction of the Fe atoms with positive V_{zz} ($p_- = 100 - p_+$), and Γ is the full width at half-maximum of elementary Lorentzian doublets.

Sample	T (K)	$\bar{\delta}$ (mm s^{-1})	$\sigma_{\bar{\delta}}$ (mm s^{-1})	$\bar{q}_+$ (mm s^{-1}) $\bar{q}_-$ (mm s^{-1})	$\sigma_{\bar{q}_+}$ (mm s^{-1}) $\sigma_{\bar{q}_-}$ (mm s^{-1})	$\bar{q}_+/\sigma_{\bar{q}_+}$ $\lvert\bar{q}_-\rvert/\sigma_{\bar{q}_-}$	$\bar{\eta}$	p_+ (%)	Γ (mm s^{-1})
i-$Al_{55}Si_7Cu_{25.5}Fe_{12.5}$	5.5	0.1164(79)	0.0230(42)	0.3716(448)	0.2549(156)	1.458(265)	0.0(3)	52.1(1.1)	0.2899(9)
				−0.3646(294)	0.2039(315)	1.788(454)			
1/1 approximant	5.4	0.0882(51)	0.0569(71)	0.2917(92)	0.1209(178)	2.409(431)	0.0(2)	62.3(1.3)	0.2619(8)
$Al_{55}Si_7Cu_{25.5}Fe_{12.5}$				−0.3629(164)	0.1604(207)	2.262(394)			
i-$Al_{62.5}Cu_{24.5}Fe_{13}$	4.4	0.0985(32)	0.0759(84)	0.3683(150)	0.1473(216)	2.500(476)	0.0(2)	48.5(9)	0.2470(7)
				−0.3845(144)	0.1738(159)	2.212(286)			

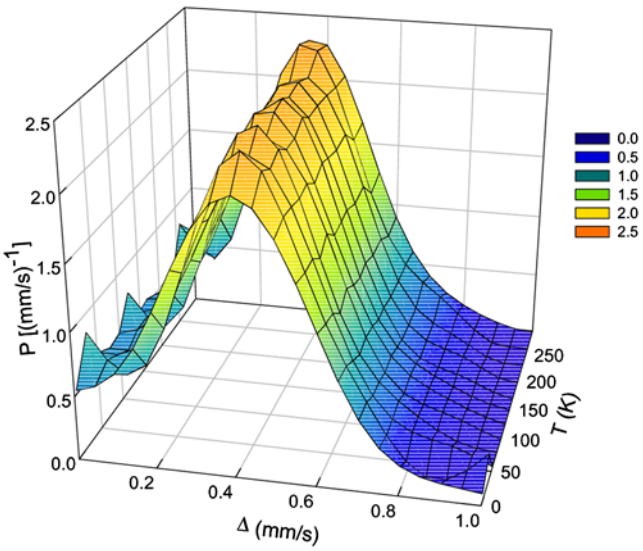

Figure 6. A 3D projection of the $P(\Delta)$ distribution for i-$Al_{62.5}Cu_{24.5}Fe_{13}$.

bimodal character of $P(q)$, found experimentally (figure 5(d)), and thus it is closer to the true structural model of i-Al–Cu–Fe.

Distributions $P(\Delta)$ similar to those in figure 4(d) were determined from the fits of the i-$Al_{55}Si_7Cu_{25.5}Fe_{12.5}$ alloy, its 1/1 approximant, and i-$Al_{62.5}Cu_{24.5}Fe_{13}$ measured at other temperatures. Figure 6 shows such distributions for the i-$Al_{62.5}Cu_{24.5}Fe_{13}$ alloy. One can note the decrease of $\bar{\Delta}$ with increasing temperature. The temperature dependence of $\bar{\Delta}$ could be fitted (figure 7) to the empirical equation

$$\bar{\Delta}(T) = \bar{\Delta}(0)(1 - BT^{3/2}), \tag{2}$$

where $\bar{\Delta}(0)$ is the value of $\bar{\Delta}$ at 0 K and B is a constant. Such a $T^{3/2}$ temperature dependence has been observed in many metallic noncubic crystalline alloys [29], in some amorphous [30, 31] alloys, and recently in i alloys [31, 32] over temperature ranges from a few K to the melting point. This seemingly universal $T^{3/2}$ dependence is not well understood. Its origin seems to be associated with a strong temperature dependence of mean square lattice displacements and, to a lesser extent, with the temperature dependence of the lattice expansion [33]. The values of $\bar{\Delta}(0)$, B determined from the fits for i-$Al_{55}Si_7Cu_{25.5}Fe_{12.5}$, its 1/1 approximant, and i-$Al_{62.5}Cu_{24.5}Fe_{13}$ are, respectively, 0.4051(11) mm s^{-1}, 7.84(54) $\times$ 10^{-6} K$^{-3/2}$, 0.3627(6) mm s^{-1}, 6.85(36) $\times$ 10^{-6} K$^{-3/2}$, and 0.3939(6) mm s^{-1}, 10.2(4) $\times$ 10^{-6} K$^{-3/2}$. It can be concluded that although the temperature dependences of $\bar{\Delta}$ in i-$Al_{55}Si_7Cu_{25.5}Fe_{12.5}$ and its 1/1 approximant are the same within the experimental error, the values of $\bar{\Delta}$ are significantly different. A stronger temperature dependence of $\bar{\Delta}$ is found in i-$Al_{62.5}Cu_{24.5}Fe_{13}$, and the values of $\bar{\Delta}$ are close to those for i-$Al_{55}Si_7Cu_{25.5}Fe_{12.5}$. The values of $\bar{\Delta}$ being larger for the i alloys than the 1/1 approximant indicates the presence of more topological disorder in the former than in the latter.

The average centre shift at temperature T, $\bar{\delta}(T)$, determined from the fits of the spectra of the samples studied is given by

$$\bar{\delta}(T) = \delta_0 + \delta_{SOD}(T), \tag{3}$$

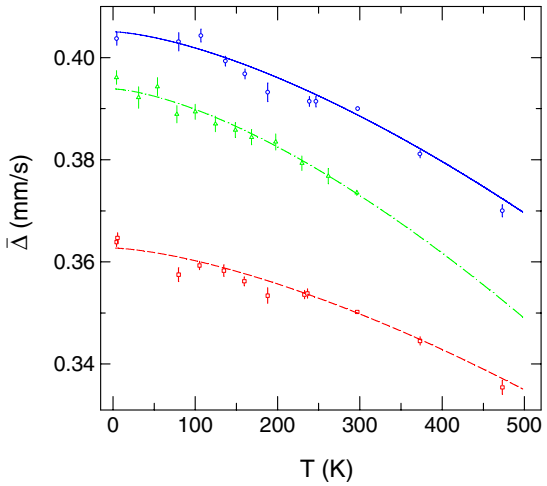

Figure 7. The temperature dependence of the average quadrupole splitting of i-$Al_{55}Si_7Cu_{25.5}Fe_{12.5}$ (open circles), its 1/1 approximant (open squares), and i-$Al_{62.5}Cu_{24.5}Fe_{13}$ (open triangles). The solid, dashed, and dot–dashed lines are the fits to equation (2), as explained in the text.

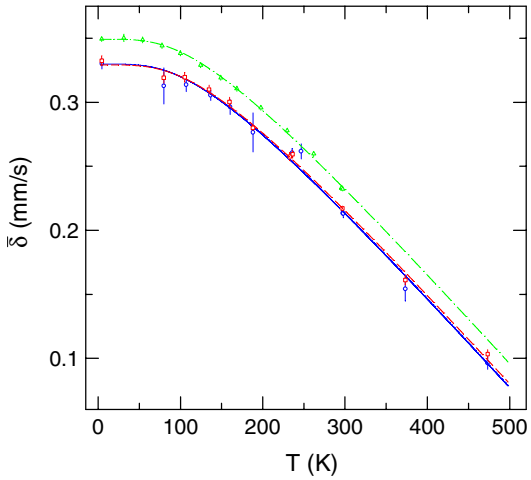

Figure 8. The temperature dependence of the average centre shift of i-$Al_{55}Si_7Cu_{25.5}Fe_{12.5}$ (open circles), its 1/1 approximant (open squares), and i-$Al_{62.5}Cu_{24.5}Fe_{13}$ (open triangles). The solid, dashed, and dot–dashed lines are the fits to equation (3), as explained in the text.

where δ_0 is the intrinsic isomer shift and $\delta_{SOD}(T)$ is the second-order Doppler (SOD) shift which depends on the lattice vibrations of the Fe atoms [12]. In terms of the Debye approximation of the lattice vibrations, $\delta_{SOD}(T)$ is expressed [34] in terms of the characteristic Mössbauer temperature Θ_M (Θ_M is distinct from the Debye temperature, Θ_D, determined from specific heat measurements, which is based on a different weight of the phonon frequency distribution [34]) as

$$\delta_{SOD}(T) = -\frac{9}{2}\frac{k_B T}{Mc}\left(\frac{T}{\Theta_M}\right)^3 \int_0^{\Theta_M/T} \frac{x^3\,dx}{e^x - 1}, \tag{4}$$

where M is the mass of the Mössbauer nucleus and c is the speed of light. By fitting the experimental data $\bar{\delta}(T)$ (figure 8) to equation (4), the quantities δ_0 and Θ_M can be

determined. They are 0.3285(43) mm s^{-1}, 484(34) K, 0.3292(25) mm s^{-1}, 487(19) K, and 0.3492(8) mm s^{-1}, 466(7) K, respectively, for i-$Al_{55}Si_7Cu_{25.5}Fe_{12.5}$, its 1/1 approximant, and i-$Al_{62.5}Cu_{24.5}Fe_{13}$.

The values of δ_0 are the same within the experimental error for i-$Al_{55}Si_7Cu_{25.5}Fe_{12.5}$ and its 1/1 approximant, and smaller than those for i-$Al_{62.5}Cu_{24.5}Fe_{13}$. As δ_0 is the measure of the s electron density at the Mössbauer nucleus [12], the values of δ_0 being the same indicates that the electronic properties of i-$Al_{55}Si_7Cu_{25.5}Fe_{12.5}$ and its 1/1 approximant are very similar.

Once Θ_M is known, the Lamb–Mössbauer factor at any temperature can be determined from

$$f(T) = \exp\left\{-\frac{3E_\gamma^2}{Mc^2k_B\Theta_M}\left[1+4\left(\frac{T}{\Theta_M}\right)^2\int_0^{\Theta_M/T}\frac{x\,dx}{e^x-1}\right]\right\}, \tag{5}$$

where E_γ is the energy of the Mössbauer γ-ray transition. The values of f at room temperature (297.2 K) for i-$Al_{55}Si_7Cu_{25.5}Fe_{12.5}$, its 1/1 approximant, and i-$Al_{55}Si_7Cu_{25.5}Fe_{12.5}$ are, respectively, 0.823(23), 0.825(12), and 0.811(5). The values of f being the same implies that on average the Fe atoms are bound in the same way in all the alloys studied.

3.3. Electrical resistivity

The temperature dependence of the electrical resistivity $\rho(T)$ and the normalized resistivity $\rho(T)/\rho_{300\ K}$ in the i-$Al_{62.5}Cu_{24.5}Fe_{13}$ alloy and the $Al_{55}Si_7Cu_{25.5}Fe_{12.5}$ 1/1 approximant are shown in figure 9. Both compounds possess a negative temperature coefficient of electrical resistivity (TCR) over a wide temperature range from 20 to 300 K. The negative TCR strongly suggests the presence of quantum interference effects, the weak-localization and electron–electron interactions, that occur in QCs [35, 36]. A decrease in the electrical resistivity below 20 K observed in both phases is also understood within the framework of the weak-localization theory, provided that the scattering event associated with magnetic impurities takes place in these compounds.

The residual resistivity ratio RRR $= \rho_{2\,K}/\rho_{300\,K}$ for the i-$Al_{62.5}Cu_{24.5}Fe_{13}$ alloy being larger than that for the 1/1 approximant indicates a stronger localization tendency in the i phase. We consider that the strong localization tendency would be closely related to a small density of states at the Fermi level (E_F). The small density of states at E_F indicates small Fermi surface(s). In the case with small Fermi surfaces, multiple elastic scattering easily satisfies the condition for quantum interference. Once the Fermi surfaces get larger, the quantum interference effect should be weakened because an inelastic event appears before the multiple scattering satisfies the condition. This is illustrated schematically in figure 10. Further evidence for the smaller density of states in the i phase is reflected in the value of $\rho_{300\ K}$, which will be discussed later.

Since the weak localization is caused by multiple elastic scattering associated with heavily disordered or aperiodic structures, one may wonder whether the crystalline approximants of a periodic structure should stay far away from the weak-localization effect. We should note here, however, that chemical and structure disorder do exist in the $Al_{55}Si_7Cu_{25.5}Fe_{12.5}$ 1/1 approximant, as was clearly determined in the present Rietveld analysis. Thus this disordering must be responsible for the increase of ρ with decreasing temperature in the approximant. It was reported that the structure of other 1/1 approximants exhibiting high ρ was also characterized by chemical and structure disorder, and that a negative TCR was observed in these approximants [17, 36, 37].

Quantum interference effects are known to be weakened as inelastic scattering increases with increasing temperature. If the temperature is high enough to completely destroy the quantum interference, then the weak localization disappears. In such a case, the electrical

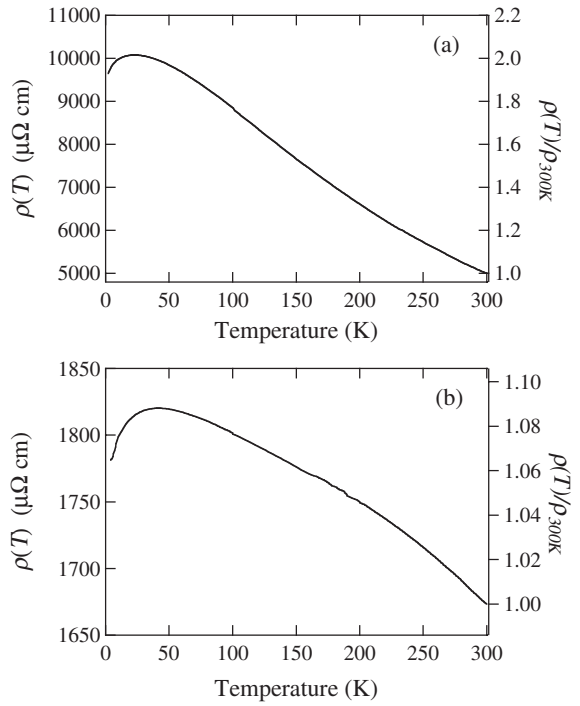

Figure 9. The electrical resistivity of (a) i-$Al_{62.5}Cu_{24.5}Fe_{13}$ and (b) the 1/1 approximant $Al_{55}Si_7Cu_{25.5}Fe_{12.5}$.

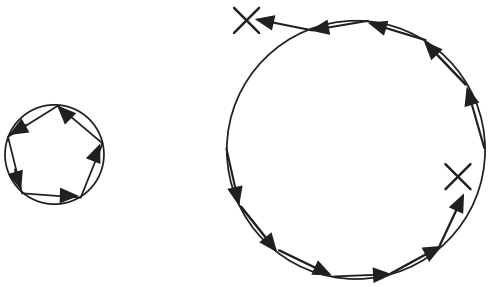

Figure 10. A schematic drawing of the multiple elastic scattering on small and large Fermi surfaces. On the small Fermi surface, multiple elastic scattering easily satisfies the condition for quantum interference. The condition for quantum interference with the large Fermi surface, on the other hand, is difficult to satisfy, because inelastic scattering would be introduced and would destroy the quantum interference before the multiple elastic events caused rounding of the Fermi surface. When the Fermi surface is large enough, quantum interference never appears, even though the number of inelastic events is much smaller than the number of elastic events.

resistivity is explained by the ordinary Boltzmann transport formula with a restricted mean free path $\lambda \approx a$, where a represents the averaged inter-atomic distances [38]. This condition is widely known as the Ioffe–Regel limit [39]. The large electrical resistivity, exceeding 1600 $\mu\Omega$ cm at room temperature, therefore, indicates a small density of states at E_F. The negative TCR constitutes clear evidence that the Ioffe–Regel limit has been reached. Note that since λ has already been saturated below the Ioffe–Regel limit, chemical and structural

disorder, which are expected to shorten λ, no longer contribute to the enhancement of the electrical resistivity.

The value of ρ for the i-$Al_{62.5}Cu_{24.5}Fe_{13}$ alloy is almost twice that for the 1/1 approximant at room temperature. This is most probably due to the density of states at E_F in the i-$Al_{62.5}Cu_{24.5}Fe_{13}$ alloy being smaller than that in the $Al_{55}Si_7Cu_{25.5}Fe_{12.5}$ 1/1 approximant because the evolution of ρ in these phases is determined by the weak localization and the Boltzmann equation under the Ioffe–Regel limit, both of which are developed by the small density of states at E_F, as described above. The formation of a pseudogap at E_F is one of the most salient characteristics of i QCs, and it is frequently discussed in terms of the Fermi sphere–Brillouin zone (FS–BZ) interaction [40]. A nearly spherical symmetry in the i phase would produce a nearly spherical quasi-Brillouin zone. A spherical Fermi surface contacts with the nearly spherical quasi-Brillouin zone at many different wave points in the reciprocal space of the extended zone scheme. As a result, a deeper pseudogap than that in the 1/1 approximant is produced in the i QC. Thus, the symmetrical nature of i QCs contributes to enhancement of their ρ by reducing their density of states at E_F with the FS–BZ interaction. The quasiperiodic order in QCs, on the other hand, does not lead to enhancement of their ρ which exhibits essentially the same behaviour as in the heavily disordered materials.

4. Conclusions

The structure of the 1/1 approximant $Al_{55}Si_7Cu_{25.5}Fe_{12.5}$ has been refined. The distribution in sign of the principal component of the EFG tensor and the average value of the asymmetry parameter have been determined. The local order of the Fe structural environment is compared in the i-$Al_{55}Si_7Cu_{25.5}Fe_{12.5}$ alloy, its 1/1 approximant, and the i-$Al_{62.5}Cu_{24.5}Fe_{13}$ alloy. The temperature dependence of the average quadrupole splitting follows the $T^{3/2}$ dependence characteristic for metallic alloys. The lattice vibrations of the Fe atoms in the alloys studied are well described by a Debye model with the characteristic Mössbauer temperatures of 484(34), 487(19), and 466(7) K. No unusual properties which could be associated with quasiperiodic nature of the i alloys $Al_{55}Si_7Cu_{25.5}Fe_{12.5}$ and $Al_{62.5}Cu_{24.5}Fe_{13}$ have been found.

Acknowledgment

This work was supported by the Natural Sciences and Engineering Research Council of Canada.

References

[1] Stadnik Z M (ed) 1999 *Physical Properties of Quasicrystals* (Berlin: Springer)
[2] Edagawa K, Naito N and Takeuchi S 1992 *Phil. Mag.* B **65** 1011
[3] Mayou D, Berger C, Cyrot-Lackmann F, Klein T and Lanco P 1993 *Phys. Rev. Lett.* **70** 3915
[4] Berger C, Gignoux C, Tjernberg O, Lindqvist P, Cyrot-Lackmann F and Calvayrac Y 1995 *Physica* B **204** 44
[5] Hippert F, Brand R A, Pelloth J and Calvayrac Y 1994 *J. Phys.: Condens. Matter* **6** 11189
[6] Brand R A, Pelloth J, Hippert F and Calvayrac Y 1994 *Hyperfine Interact.* **94** 2249
[7] Hippert F, Brand R A, Pelloth J and Calvayrac Y 1995 *Proc. 5th Int. Conf. on Quasicrystals* ed C Janot and R Mosseri (Singapore: World Scientific) p 464
[8] Brand R A, Pelloth J, Hippert F and Calvayrac Y 1998 *Aperiodic '97: Proc. Int. Conf. on Aperiodic Crystals* ed M de Boissieu, J-L Verger-Gaugry and R Currat (Singapore: World Scientific) p 745
[9] Quivy A, Quiquandon M, Calvayrac Y, Faudot F, Gratias D, Berger C, Brand R A, Simonet V and Hippert F 1996 *J. Phys.: Condens. Matter* **8** 4223
[10] Izumi F 1993 *The Rietveld Method* ed R A Young (Oxford: Oxford University Press) p 236
[11] Cali J P (ed) 1971 Certificate of calibration *Iron Foil Mössbauer Standard* NBS Circular No 1541 (Washington, DC: US Government Printing Office)

[12] Greenwood N N and Gibb T C 1971 *Mössbauer Spectroscopy* (London: Chapman and Hall)
Gütlich P, Link R and Trautwein A 1978 *Mössbauer Spectroscopy and Transition Metal Chemistry* (Berlin: Springer)
[13] Cooper M and Robinson K 1966 *Acta Crystallogr.* **20** 614
[14] Takeuchi T, Yamada H, Takata M, Nakata T, Tanaka N and Mizutani U 2000 *Mater. Sci. Eng.* **294–296** 340
[15] Puyraimond F, Quiquandon M, Gratias D, Tillard M, Belin C, Quivy A and Calvayrac Y 2002 *Acta Crystallogr.* A **58** 391
Puyraimond F, Tillard M, Belin C, Quiquandon M, Gratias D, Quivy A and Calvayrac Y 2001 *Ferroelectrics* **250** 281
[16] Yamada H, Takeuchi T, Mizutani U and Tanaka N 1999 *MRS Symp. Proc.* **553** 117
[17] Takeuchi T and Mizutani U 2002 *J. Alloys Compounds* **342** 416
[18] Stadnik Z M 1996 *Mössbauer Spectroscopy Applied to Magnetism and Materials Science* vol 2, ed G J Long and F Grandjean (New York: Plenum) p 125
[19] Le Caër G and Dubois J M 1979 *J. Phys. E: Sci. Instrum.* **12** 1083
[20] Hesse J and Rübartsch A 1974 *J. Phys. E: Sci. Instrum.* **7** 526
[21] Blaes N, Fischer H and Gonser U 1985 *Nucl. Instrum. Methods Phys. Res.* B **9** 201
[22] Le Caër G and Brand R A 1998 *J. Phys.: Condens. Matter* **10** 10715
[23] Gratias D, Puyraimond F, Quiquandon M and Katz A 2001 *Phys. Rev.* B **63** 024202 and references therein
[24] Blaha P, Schwartz K, Faber W and Luitz J 2000 *Hyperfine Interact.* **126** 389
[25] Kramer P, Quandt A, Schlottmann M and Schneider T 1995 *Phys. Rev.* B **51** 8815
Kramer P, Quandt A, Schneider Th and Teucher H 1997 *Phys. Rev.* B **55** 8793
Kramer P, Quandt A, Schneider Th and Teucher H 1998 *Phys. Rev.* B **57** 5542 (erratum)
[26] Zijlstra E S, Kortus J, Krajčí M and Bose S K 2003 *Phys. Rev.* B submitted
[27] Cockayne E, Phillips R, Kan X B, Moss S C, Robertson J L, Ishimasa T and Mori M 1993 *J. Non-Cryst. Solids* **153/154** 140
[28] Kan X B, Robertson J L, Moss S C, Kulik J, Ishimasa T, Mori M, Quivy A, Gratias D, Elser V and Zschack P 1993 *J. Non-Cryst. Solids* **153/154** 33
[29] Kaufmann E N and Vianden R J 1979 *Rev. Mod. Phys.* **51** 161 and references therein
[30] Deppe P and Rosenberg M 1983 *Hyperfine Interact.* **15/16** 735
Kopcewicz M, Kopcewicz B and Gonser U 1987 *J. Magn. Magn. Mater.* **66** 79
Mao M, Ryan D H and Altounian Z 1994 *Hyperfine Interact.* **92** 2163
[31] Stadnik Z M, Saida J and Inoue A 2001 *Ferroelectrics* **250** 297
Stadnik Z M, Rapp Ö, Srinivas V, Saida J and Inoue A 2002 *J. Phys.: Condens. Matter* **14** 6883
[32] Stadnik Z M, Takeuchi T and Mizutani U 2000 *Mater. Sci. Eng.* A **294–296** 331
Brand R A, Voss J and Calvayrac Y 2000 *Mater. Sci. Eng.* A **294–296** 666
[33] Jena P 1976 *Phys. Rev. Lett.* **36** 418
Nishiyama K, Dimmling F, Kornrumph Th and Riegel D 1976 *Phys. Rev. Lett.* **37** 357
Christiansen J, Heubes P, Keitel R, Klinger W, Loeffler W, Sandner W and Witthuhn W 1976 *Z. Phys.* B **24** 177
[34] Kolk B 1984 *Dynamical Properties of Solids* vol 5, ed G K Horton and A A Maradudin (Amsterdam: North-Holland) p 3
De Grave E, Verbeeck A E and Chambaere D G 1985 *Phys. Lett.* A **107** 181
[35] Rapp Ö 1999 *Physical Properties of Quasicrystals* ed Z M Stadnik (Berlin: Springer) p 127
[36] Takeuchi T, Banno E, Onogi T, Mizuno T, Sato T, Fournée V and Mizutani U 2001 *MRS Symp. Proc.* **643** K13.4.1
[37] Onogi T, Takeuchi T, Sato H and Mizutani U 2002 *J. Alloys Compounds* **342** 397
[38] Kaveh M and Mott N F 1983 *Phil. Mag.* B **47** L9
[39] Mott N F 1990 *Metal–Insulator Transitions* 2nd edn (London: Taylor and Francis)
[40] Sato H, Takeuchi T and Mizutani U 2001 *Phys. Rev.* B **64** 094207